Supplementary File for

Coseismic and Early Postseismic Deformation Mechanism Following the 2021 Mw 7.4 Maduo Earthquake: Insights from Satellite Radar Interferometry and GPS

Chuanzeng Shu [1], Zhiguo Meng [1,*], Qiong Wu [1], Wei Xiong [2], Lijia He [3], Xiaoping Zhang [4], and Dan Xu [5]

[1] College of Geoexploration Science and Technology, Jilin University, Changchun 130026, China; shucz22@mails.jlu.edu.cn (C.S.); mengzg@jlu.edu.cn (Z.M.); wuqiong@jlu.edu.cn (Q.W.)
[2] Key Laboratory of Earthquake Geodesy, Institute of Seismology, China Earthquake Administration, Wuhan 430071, China; xiongwei@cgps.ac.cn (W.X.)
[3] Laboratory of Radar Remote Sensing, School of Geosciences and Info-Physics, Central South University, Changsha 410083, China; lijiahe@csu.edu.cn (L.H.)
[4] State Key Laboratory of Lunar and Planetary Sciences, Macau University of Science and Technology, Macau 999078, China; xpzhang@must.edu.mo (X.Z.)
[5] Changbai Mountain Tianchi Volcano Observatory, Antu 133618, China; dxu8123@gmail.com (D.X.)
* Correspondence: mengzg@jlu.edu.cn

Contents of this file

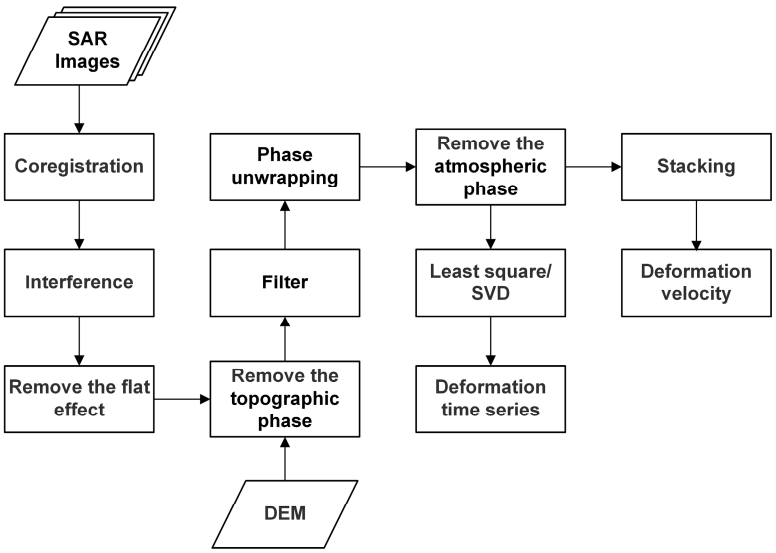

Figure S1. The processing flowchart of SBAS-InSAR and Stacking-InSAR methods.

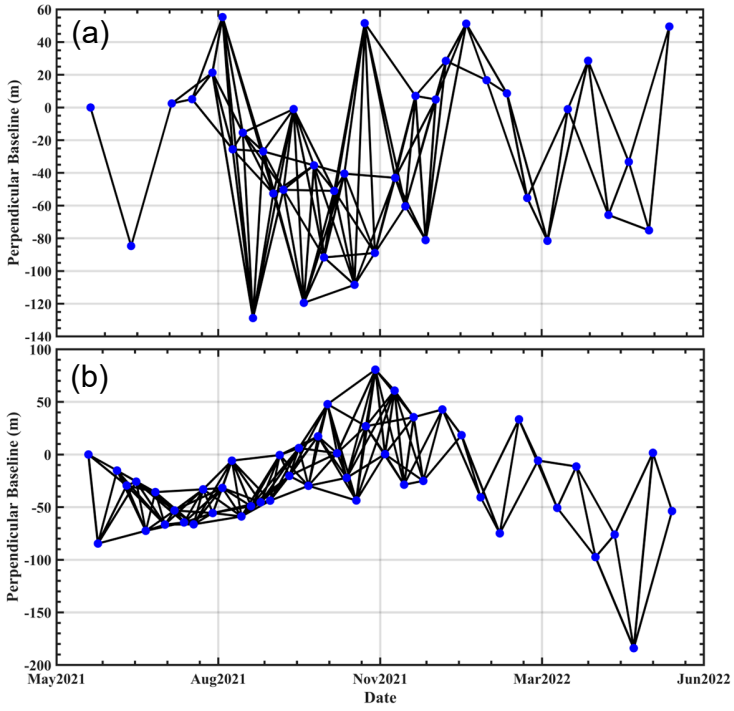

Figure S2. The distribution combination of interference pairs from ascending orbit 99 (a) and descending orbit 106 (b).

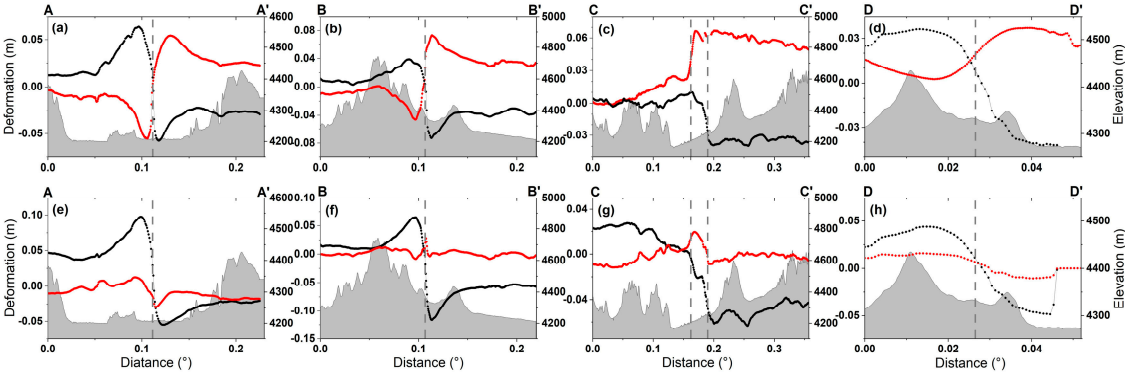

Figure S3. Deformation profiles (a)–(h) along measuring lines A–A', B–B', C–C', and D–D' spanning seismogenic fault. The gray vertical dashed line represents the location of the seismogenic fault, while the gray contour represents the topographic relief. In subgraphs (a)–(d), the red dots are collected from the LOS deformation map of the ascending orbit (see Figure 4c), and the black dots are collected from the LOS deformation map of the descending orbit (see Figure 4g). In subgraphs (e)–(h), the red dots are collected from the 2.5-D quasi-EW deformation map (see Figure 7c) and the black dots are collected from the 2.5-D quasi-vertical deformation map (see Figure 7g). The deformation values in the quasi-E and the quasi-upward directions are positive.

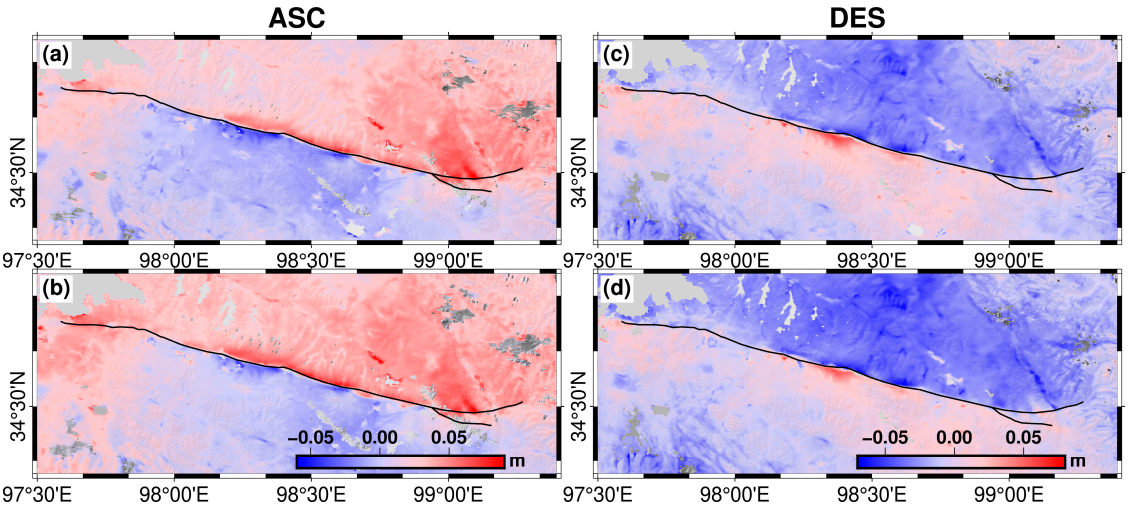

Figure S4. (a) and (c) represent the deformation observed by InSAR, while (b) and (d) represent the deformation after removing the effects of viscoelastic relaxation and poroelastic rebound.

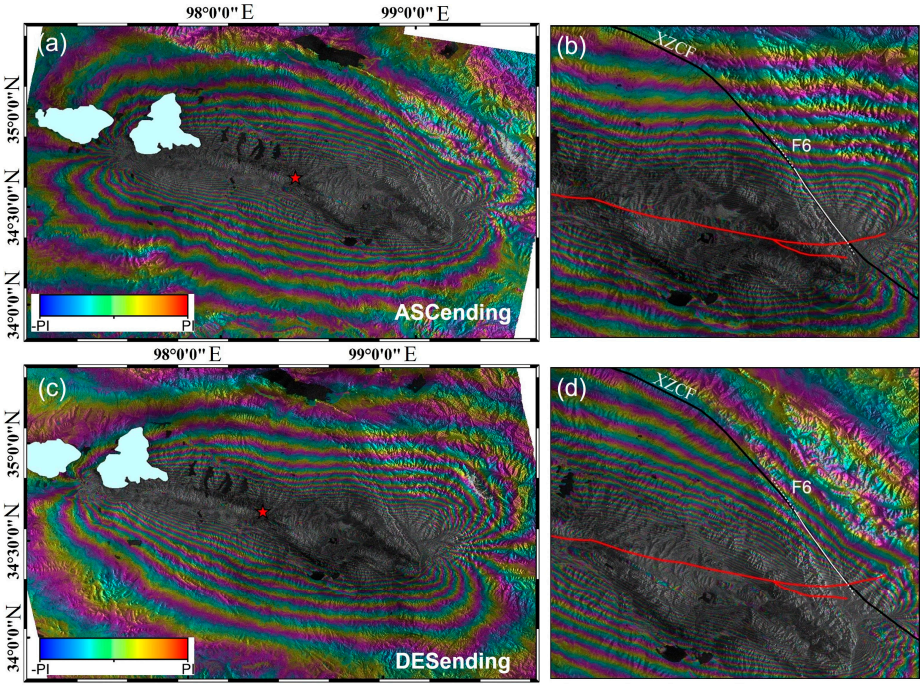

Figure S5. D-InSAR interferograms (20210520–20210526) from the ascending (a, b) and descending (c, d) orbits of the Maduo event. Each subplot was rendered with 50% transparency. F6 represents the fault reactivated by the Maduo event, and the white dashed line represents the inferred fault segment based on the deformation signal.

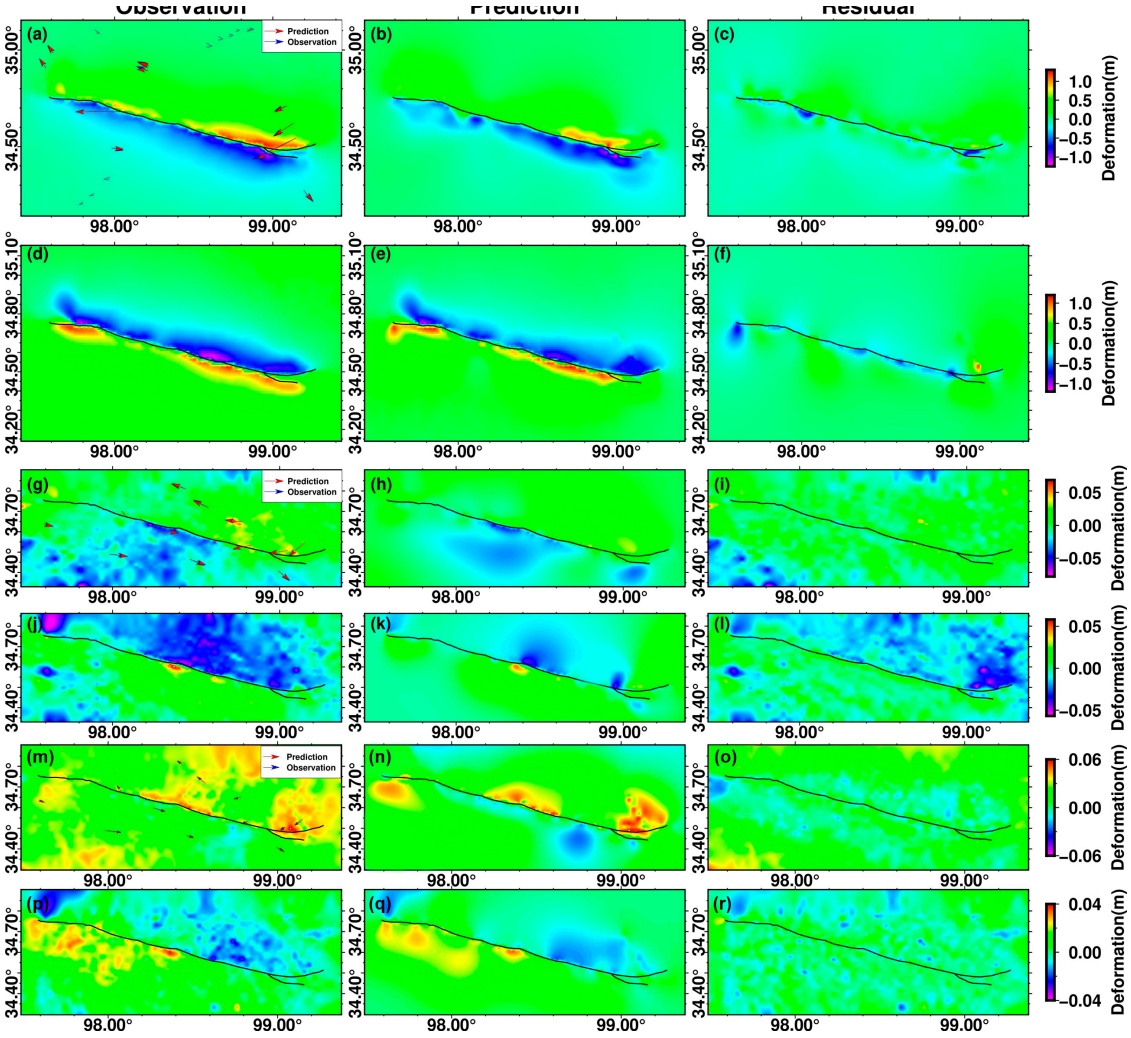

Figure S6. Observed displacements (a, d, g, j, m, and p), best-fit model predictions (b, e, h, k, n, and q), and residuals (c, f, i, l, o, and r) in coseismic and postseismic (the early stage and 1 year) slip models. The (a) and (d) represent the D-InSAR deformation from the ascending and descending orbits used for the inversion of coseismic slip. Similarly, (g) and (j) represent one year after the mainshock, while (m) and (p) represent the early stage after the mainshock. The arrows in subgraphs (a) (m), and (g) represent GPS displacements that constrain coseismic and postseismic (the early stage and 1 year) slip, respectively.

Table S1. SAR data and GPS Stations used in co- and postseismic observations.

Sensor	Track	Pass	Acquisition time (yyyymmdd)	Track	Pass	Acquisition time (yyyymmdd)	GPS Stations (Coseismic)	GPS Stations (Postseismic)
Sentinel-A/B	99	Ascending	20210526	106	Descending	20210526	4432	2836
			20210619			20210601	4441	2840
			20210713			20210613	4447	4454
			20210725			20210619	4452	4499
			20210806			20210625	4454	J406
			20210812			20210701	4495	JDUO
			20210818			20210707	4499	KANQ
			20210824			20210713	4515	MD01
			20210830			20210719	4519	MD02
			20210905			20210725	BFMQ	MD03
			20210911			20210731	BUDR	MD04
			20210917			20210806	BUJZ	MD05
			20210923			20210812	CHDU	MD07
			20210929			20210818	DLHA	MD09
			20211005			20210824	GAND	MD10
			20211011			20210830	GAZH	QHMD
			20211017			20210905	GCHA	
			20211023			20210911	GERM	
			20211029			20210917	GSMA	
			20211104			20210923	HAIY	
			20211110			20210929	HMHE	
			20211122			20211005	HSHX	
			20211128			20211011	HTTL	
			20211204			20211017	IG01	
			20211210			20211023	IG02	
			20211216			20211029	IG03	
			20211222			20211104	IG04	
			20220103			20211110	IG05	
			20220115			20211116	IG07	
			20220127			20211122	IG08	
			20220208			20211128	IG09	
			20220220			20211204	IG10	
			20220304			20211210	IG11	
			20220316			20211216	J005	
			20220328			20211222	J406	
			20220409			20220103	JDUO	
			20220421			20220115	KANQ	
			20220503			20220127	LAJA	
						20220208	LBAO	
						20220220	LOYX	
						20220304	MADU	
						20220316	MAIX	
						20220328	NANQ	
						20220409	NMUH	
						20220421	QHAE	
						20220503	QHAG	
							QHAH	
							QHAJ	

							QHBM QHDL QHGC QHGE QHMD QHMQ QHQM QHTJ QSHE TIEG WENQ XNIN XRID YANH YEGE YS20 YS21 YUSH ZHID	